Journal of Contaminant Hydrology 244 (2022) 103931

Contents lists available at ScienceDirect

Journal of Contaminant Hydrology

journal homepage: www.elsevier.com/locate/jconhyd

Evaluating dual-domain models for upscaling multicomponent reactive transport in mine waste rock

D. Pedretti [a,*], B. Vriens [b], E.K. Skierszkan [c], P. Baják [d], K.U. Mayer [e], R.D. Beckie [e]

[a] Dipartimento di Scienze della Terra "A. Desio", Università degli Studi di Milano (UNIMI), Via Mangiagalli 34, 20133 Milan, Italy
[b] Department of Geological Sciences & Engineering, Queen's University, 36 Union Street, Kingston, ON K7L 1N6, Canada
[c] Department of Geological Sciences, University of Saskatchewan, 114 Science Place, Saskatoon, SK S7N 5E2, Canada
[d] József and Erzsébet Tóth Endowed Hydrogeology Chair, Eötvös Loránd University, Budapest, Hungary
[e] Earth, Ocean and Atmospheric Sciences, University of British Columbia, 2020-2207 Main Mall, Vancouver, BC V6T 1Z4, Canada

ARTICLE INFO

Keywords:
Reactive transport modeling
Acid mine drainage
Acid rock drainage
Molybdenum
Dual porosity

ABSTRACT

Reactive transport models have proven abilities to simulate the quantity and quality of drainage from mine waste rock. Tracer experiments indicate the presence of fast and slow flow regimes in many heterogeneous waste-rock piles. Although multidomain models have been developed specifically for systems with such distinctive hydrodynamics, there have been limited applications of multidomain reactive transport models to simulate composite drainage chemistries from waste-rock piles to date. This work evaluated the ability of dual-domain multicomponent reactive transport models (DDMRTMs) to reproduce breakthrough curves of conservative (chloride) and reactive (molybdenum) solutes observed at a well-characterized experimental waste-rock pile at the Antamina Mine, Peru. We found that the DDMRTM simulations quantitatively matched eight-year-long records of conservative transport through the waste-rock pile when parameterized mainly with field-measured properties obtained from the site and limited calibration. The DDMRTM model also provided a reasonable match to field observations of the reactive solute. The limited calibrated parameters are physically realistic, corroborating the ability of these multidomain models to reproduce the complex reactive-transport processes governing polluted rock drainage from large-scale waste-rock piles.

1. Introduction

Waste-rock piles (WRPs) are large, heterogeneous structures that contain mine waste rock and below-grade ore. The weathering of waste rock can generate poor-quality drainage, i.e., alkaline, circum-neutral or acidic seepage with elevated metal(loid) concentrations, for many decades after construction or mine closure. Predictions of the quantity and quality of this mine drainage, including flow rates and geochemical compositions, are needed to make reliable mine-waste management decisions and to limit environmental impact (Blowes et al., 2003; Sracek et al., 2004; Wolkersdorfer et al., 2020). Multicomponent reactive transport models (MRTMs) are established tools for simulating the release of polluted mine drainage from waste rock (Gerke et al., 1998; Molson et al., 2012; Fala et al., 2013; Lahmira et al., 2016; Muniruzzaman and Pedretti, 2020), and to assist industry and government stakeholders with mine waste and wastewater management during the entire mining lifecycle.

The development and parameterization of MRTMs for WRPs is complicated by the physical and mineralogical heterogeneities within these piles (Gerke et al., 1998; Nichol et al., 2005; Demers et al., 2013; Fala et al., 2013). Waste-rock grain sizes can range over multiple orders of magnitude — from clay to boulders — and pile construction methods affect the mixing and segregation of units with different textural and compositional properties (Price, 2009; INAP-GARD, 2014). As with many heterogeneous systems, the field-scale information needed to parameterize this heterogeneity at industry-relevant scales (i.e. hundreds of meters tall waste-rock piles) is limited, resulting in uncertain model predictions (Pedretti et al., 2017, 2020). Furthermore, even if all model parameters could be hypothetically characterized at the pore scale of a full-scale WRP, which contains thousands of m^3 of waste rock, the resulting fully-parameterized MRTM would be computationally prohibitive to resolve, as multiple nonlinearly coupled processes are implicated in the prediction of WRPs drainage quantity and quality (Amos et al., 2015).

* Corresponding author.
E-mail address: daniele.pedretti@unimi.it (D. Pedretti).

https://doi.org/10.1016/j.jconhyd.2021.103931
Received 15 August 2021; Received in revised form 19 October 2021; Accepted 19 November 2021
Available online 23 November 2021

Upscaled models have been increasingly used in hydrogeological applications as computationally efficient "surrogates" of more complex models (Neuman and Tartakovsky, 2009; Asher et al., 2015; Fiori et al., 2015). The dual-domain model (DDM), also sometimes referred to as a dual-porosity or mobile-immobile model, is an example of a widely adopted upscaled model. It has been developed for modeling flow and transport in heterogeneous porous media with low and high permeability zones (Simunek et al., 2003; Zheng et al., 2011). The DDM approach (Fig. 1) represents the high- and low-permeability system as a continuum comprised of two domains or *porosities* at every point. The *mobile* porosity (θ_m) is characterized by a much shorter solute residence time than in the *immobile* porosity (θ_{im}). Advection occurs solely in the mobile domain. Water and solutes are exchanged between the mobile and immobile porosities by means of non-equilibrium (i.e., kinetic) mass transfer. The DDM representation is well-suited to describe solute transport in systems with bimodal distributions of water residence times, e.g., porous media with well-defined contrasts in hydraulic conductivity or fractured aquifers (Hadermann and Heer, 1996; Pedretti et al., 2014; Molinari et al., 2015).

Dual-domain models have proven useful to describe the behavior of flow and conservative tracers in WRPs (Blackmore et al., 2018). However, they have rarely been applied to reactive transport simulations of leachate composition from WRPs, in particular for multicomponent simulations, despite the heterogeneity of hydraulic conductivities intrinsic to WRPs. One possible reason for this paucity is that the parameters of upscaled models, such as the mass-transfer rates of dual-domain models, are difficult to constrain experimentally. This is true for reactive solutes and full-scale heterogeneous WRPs, but even for non-reactive solutes in well-controlled theoretical studies and laboratory experiments (Donado et al., 2009; Willmann et al., 2010; Molinari et al., 2015).

In this work, we evaluated the ability of a dual-domain multicomponent reactive transport model (DDMRTM) to predict long-term records of neutral rock drainage (NRD) from a well-studied experimental WRP at the Antamina Mine in Peru (Conlan et al., 2012; Lorca et al., 2016; Skierszkan et al., 2016; Vriens et al., 2019c, 2019a, 2019b). Our goal was to analyze in detail the parameterization of our model and determine whether a DDMRTM can be a useful upscaled modeling approach that is able to predict NRD with limited empirical fitting of model parameters. In the analyzed experimental pile, reactive species were mobilized under circumneutral pH conditions (Vriens et al., 2019c). The breakthrough curves (BTCs) of reactive and conservative solutes provide a dataset well suited to assess the capabilities of our DDMRTM to simulate NRD generation and release.

The adopted methodology can be summarized as follows. First, we performed a forward-modeling analysis to reproduce flow and conservative transport in the studied pile. The adopted non-calibrated parameters were obtained from previous dual-domain modeling analyses (Blackmore et al., 2018) targeting conservative transport in other experimental piles with similar geometrical, textural and compositional characteristics. This allowed us to evaluate if empirical parameters obtained for similar piles are useful to make predictions on others. Then, the conservative transport model was upgraded to a reactive transport model, making this a novel contribution compared to the previous upscaling modeling analysis for waste rock, which focused exclusively on conservative transport. We constrained the incorporated geochemical reactions a-priori through a selection of kinetic parameters from the literature and existing field data from the studied site. Only one parameter, the kinetic rate of molybdenite oxidation, was treated as fitting parameter. A sensitivity analysis was performed to evaluate the controls of the key parameters on the model outputs.

2. Materials and methods

2.1. Site overview and experimental data

The Antamina mine in Peru hosts one of the world's largest experimental sites purposed for studying long-term mine waste weathering and drainage processes. Within the multi-scale research program, a signature experiment included a group of five fully instrumented mesoscale experimental WRPs (36 m × 36 m × 10 m in size; ~20,000 tons of material each) that contained different types of waste rock. Details on the analysis of rates and chemical composition of drainage from these experimental piles can be found in Vriens et al. (2019a).

Each pile was constructed in three major depositional events, i.e., end-dumped tipping phases, on top of a protective layer. Infiltrating water originating from precipitation was captured by lysimeters (Fig. 2). Each pile was underlain by three smaller sub-lysimeters of size 4 m × 4 m ("A", "B", "C") under the individual tipping phases, as well as by a large basal lysimeter spanning the bottom of the entire pile (36 m × 36 m; lysimeter "D"). In all piles, sub-lysimeters "B" were installed below the waste rock positioned closest to the bedrock and thus least exposed to fluctuations at the atmospheric boundaries. In turn, sub-lysimeters "C" captured drainage from waste rock below the frontal batter that was more sensitive to fluctuations in atmospheric conditions (Fig. 2).

Of the Antamina experimental WRPs, Pile 2 contained the most reactive and finest-grained waste rock, with a median particle diameter (D_{50}) between 9 mm and 30 mm and the 10th weight-percentile of particles (D_{10}) varying in size from <0.1 mm to 0.15 mm (Lorca et al., 2016; Vriens et al., 2019a). Very coarse material with diameter > 100 mm, expected to contribute minimally due to lower exposure of chemically reactive mineral surfaces, accounted for less than 10% of the total grain size distribution in this pile. The waste rock in the various tipping phases of Pile 2 contained mainly Class "A" rocks, the class of most reactive material produced at the site. The mineralogical composition was on average up to 2.7 wt-% pyrite, up to 2.4 wt-% chalcopyrite, and up to 0.1 wt-% molybdenite [MoS_2]. Rock Mo abundance varied roughly between 200 and 400 ppm. Carbonates comprised up to 1% of the bulk mineralogical assemblage in the pile (Vriens et al., 2019a).

The Pile 2 drainage chemistry record spans from 2007 to 2016,

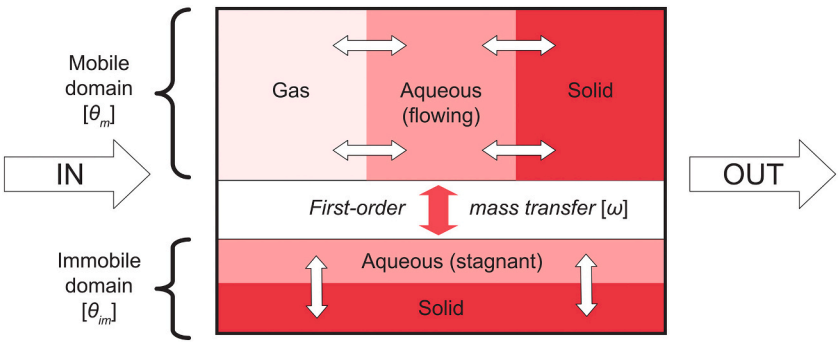

Fig. 1. Schematic illustration adapted from Cheng (2006) of the mass balance in the multiphase dual-domain model MIN3PDUAL. θ_m=mobile porosity [−]; θ_{im}=immobile porosity [−]; ω=mass-transfer rate coefficient [T^{-1}]. The model assumes that the immobile zone is fully saturated.

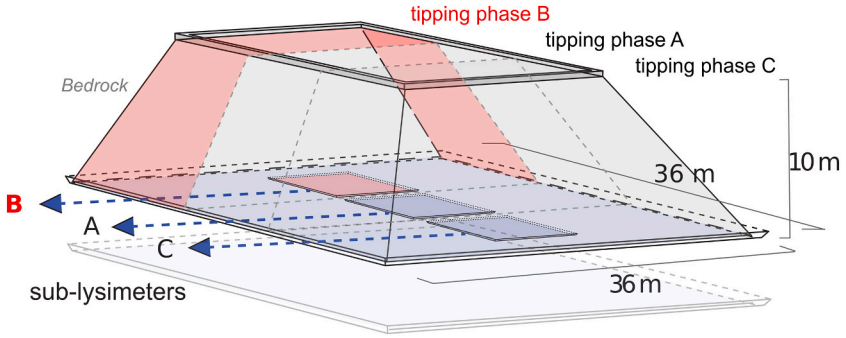

Fig. 2. Schematic illustration of the experimental waste-rock pile and the positioning of the sub-lysimeters in Experimental Pile 2 at Antamina, Peru. Adapted from Vriens et al. (2019a).

revealing that the sub-lysimeter "B" displayed characteristic features of NRD, with circumneutral pH until the end of the experiment. Part of the long-term geochemical drainage record for sub-lysimeter "B" in Pile 2 (hereafter referred to as "SL2B") is given in Fig. 3. The record reveals relatively stable circumneutral drainage pH and stable Ca and SO_4 concentrations with only minor seasonal oscillations. This behavior is explained by the fact that waste rock sampled along the flow paths arriving at SL2B contained considerable carbonate, providing a neutralizing potential ratio NPR≈2 (Lorca et al., 2016). Chloride (Cl) concentrations, a residue from blasting booster agents, drop consistently from a maximum of ~100 mgL^{-1} to a minimum of ~0.1 mgL^{-1} through time with minor oscillations. Molybdenum (Mo) concentrations rise to a maximum of ~30 mgL^{-1}, after 800–1100 days, then steadily decline to ~10 mgL^{-1} at the end of the experimental period.

2.2. Geochemical (tracer) data

The analysis of an artificial tracer test (Peterson, 2014) suggested that the flow domain in Pile 2 is mostly "matrix" flow, with mean seepage velocities estimated as 2.0–2.4 cm/day although the flow rates vary in response to rainfall events. The portion of the fluid flow following rapid, or "preferential", flow paths (open void or film flow) was a minor component (7%) of the overall flow regime. In our upscaled model, one mobile flow zone was considered to account for contributions from matrix flow and preferential flow. This mobile zone was complemented with an immobile zone in which flow rates are negligible (Fig. 1).

Dissolved Cl in the WRP drainage can be considered as an "internal conservative tracer" (Blackmore et al., 2018), rather than an externally applied conservative tracer. Chloride was released by rapid dissolution of Cl-salts from blasting residues that were imported with the waste rock during pile construction and assumed evenly distributed. As such, dissolved Cl reflects the physical transport dynamics in the WRP matrix flow domain as well as mass transfer between the immobile and mobile domain. Chloride migrated predominantly downward throughout the entire pile during weathering and drainage (Blackmore et al., 2018). Chloride transport began immediately after the pile's construction (i.e., WRP weathering *time zero*), making Cl a suitable conservative solute for the assessment of physical transport properties through SL2B.

Previous modeling by Blackmore et al. (2018) focused on Cl transport in two other experimental WRPs at Antamina, Pile 4 and Pile 5. The analysis of sub-lysimeter B of Pile 5 (hereafter, SL5B) is of specific

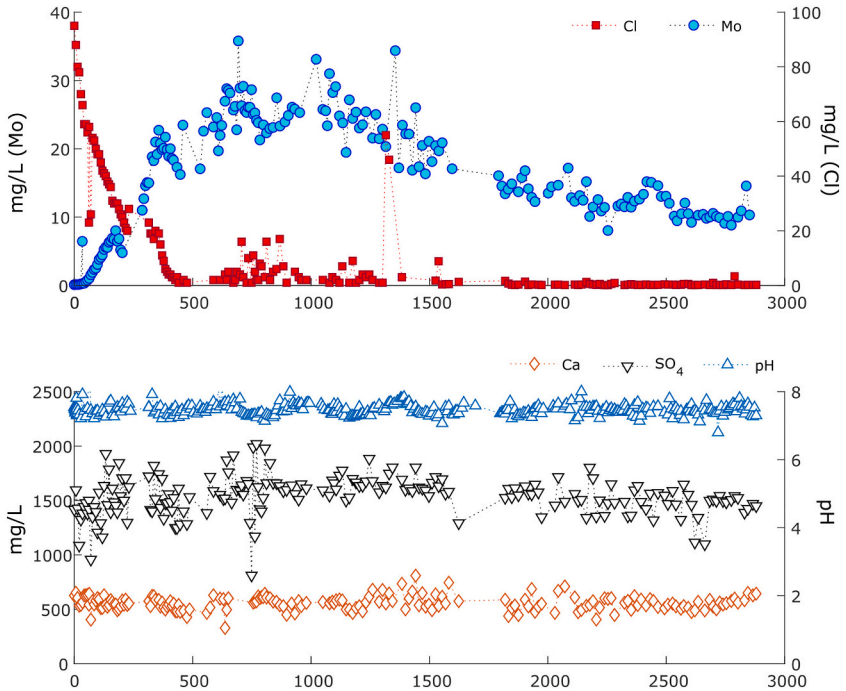

Fig. 3. Observed concentrations of Mo and Cl (top frame), as well as Ca, SO_4 and pH (bottom frame) in drainage captured by sub-lysimeter "B" from Pile 2 (SL2B). The plotted record started in 2007 and ended in 2016 (~8 years).

interest for the present study because it has similar geometry as Pile 2 and contained waste rock with comparable texture (grain size) and lithological composition, as described below. Blackmore et al. (2018) successfully reproduced Cl transport in SL5B using a similar DDM formulation. Among the key results, they found that simulating mass transfer between the mobile and immobile zones provided a superior fit of the Cl breakthrough curve (BTC) tails compared to a formulation that ignores this mass transfer. The physical processes sustaining the long-term release of contaminant from the less-mobile zones of the WRP could not be properly simulated using a 1-D single-domain conservative transport model.

In contrast to Cl, Mo is a reactive solute that can be used to test our model's capability to simulate multicomponent reactive transport within the WRP and to investigate distinct geochemical processes. Various geochemical processes relating to the mobilization and attenuation of Mo in weathering waste rock (i.e., sulfide oxidation, sorption and secondary mineral formation) have been observed at Antamina and elsewhere and have been previously parameterized, making it an excellent reactive solute for a MRTM comparison. In Antamina waste rock, aqueous Mo predominantly originates from the oxidation of molybdenite, MoS_2 (Conlan et al., 2012; Skierszkan et al., 2016; Hirsche et al., 2017). While the initial abundance of MoS_2 estimated in the pile was less than 0.1 wt-% (Vriens et al., 2019a), that amount is sufficient to generate Mo drainage levels >20 mgL^{-1}, as observed in the drainage BTC in Fig. 3. In fact, data from other Antamina field experiments similarly reveal that Mo is highly mobile under circumneutral pH drainage (Conlan et al., 2012; Skierszkan et al., 2016; Hirsche et al., 2017) with aqueous concentrations reaching >50 mgL^{-1} (Vriens et al., 2019c). Additional information on Mo primary and secondary species, speciation and Eh-pH diagrams can be found in e.g. Smedley and Kinniburgh (2017)

2.3. Modeling framework

To model conservative and reactive transport with a consistent DDMRTM framework, simulations were conducted using the code MIN3PDUAL (Cheng et al., 2004; Cheng, 2006), a dual-domain version of the multicomponent reactive transport code MIN3P (Mayer et al., 2002). MIN3PDUAL adopts the same overall structure of MIN3P but is extended with terms for secondary (immobile) porosity. The conceptual model of MIN3PDUAL is shown in Fig. 1, and the main governing equations and parameters necessary to run the simulations are presented below. Using MIN3PDUAL, we first simulated flow and conservative transport using the DDM parameters determined by Blackmore et al. (2018) on SL5B for the sub-lysimeter analyzed in this work (SL2B). Then, we extended Blackmore et al. (2018)'s conservative DDM model, incorporating multicomponent reactions to simulate the Mo BTC as well as the other BTCs relevant for the control of NRD in SL2B (Fig. 3).

2.3.1. Flow and conservative transport

Variably saturated flow in the mobile zone of MIN3PDUAL is defined in the same way as in the first release of MIN3P. There is no flow in the immobile domain which is assumed to be fully saturated with water. Flow in the mobile domain is described by Richards' equation, where fluid saturation (S), relative permeability (k_r) and pressure (defined in terms of hydraulic head, h) are related to each other by standard soil hydraulic functions (Wösten and van Genuchten, 1988). The general advection-dispersion-reaction equation for multicomponent reactive transport in the mobile (m) domain can be written as

$$\frac{\partial}{\partial t}\left(\theta_m^a T_{m,j}^a + \theta_m^g T_{m,j}^g + f T_j^s\right) = \nabla\cdot\left(\theta_m^a D^a \nabla T_{m,j}^a + \theta_m^g D^g \nabla T_{m,j}^g\right) - \nabla\cdot\left(q_a T_{m,j}^a\right) - \Gamma_j^m \quad (1)$$

where the suffixes "a", "g" and "s" represent aqueous, gaseous and sorbed phases, respectively, t is time (s), θ is the fluid content (−), T_j is the total phase component concentration ($mol{\bullet}L^{-1}$), f is the mobile porosity fraction and also the fraction of mobile sorption sites (−), D is the hydrodynamic dispersion coefficient ($m^2{\bullet}s^{-1}$), $D = \alpha_L q\theta^{-1} + D^*$, α_L is the local dispersivity (m), D^* is the effective pore water diffusion coefficient, which depends on D_w, the free diffusion coefficient in water ($m^2{\bullet}s^{-1}$) and and q is Darcy flux (for water only) ($m{\bullet}s^{-1}$). The term $\Gamma_{m,j}$ encompasses multiple sink-source terms for the j-th component, such that:

$$\Gamma_{m,j} = Q_{m,j}^{a,min} + Q_{m,j}^{ext} + Q_j^{MT} \quad (2)$$

where $Q_{m,j}^{a,min}$ represents the sink-source term due to mineral dissolution-precipitation, and $Q_{m,j}^{ext}$ represents the sink-sources terms caused by mass fluxes at the boundaries, and Q_j^{MT} represents the exchange between mobile (m) and immobile (im) domains. This last term adds the dual-domain capacity to MIN3PDUAL compared to the standard single domain version of MIN3P. The term Q_j^{MT} is defined as:

$$Q_j^{MT} = \omega\left(T_{m,j}^a - T_{im,j}^a\right) \quad (3)$$

where ω represents the first-order mass transfer rate coefficient (s^{-1}). In the immobile domain, the solute mass-balance equation is:

$$\frac{\partial}{\partial t}\left[\theta_{im}^a T_{im,j}^a + (1-f)T_j^s\right] = \Gamma_j^{im} \quad (4)$$

and:

$$\Gamma_j^{im} = Q_{im,j}^{a,m} + Q_{im,j}^{ext} + Q_j^{MT} \quad (5)$$

noticing that the dual-domain advection-dispersion model approaches the single domain equivalent as $\omega \to 0$. It was assumed that the mass-transfer term ω is ion-independent, i.e., the same for all aqueous components.

Key input parameters used in the transport model are listed in Table 1. The vertically oriented 1-D model was set to reproduce the 10-m-tall waste-rock column above SL2B, discretized into 100 control volumes. Second-type (Neumann) boundary conditions were adopted to simulate the net recharge at the top of the pile. Basal exfiltration from the pile was simulated as a seepage boundary, which also acts as a free-exit boundary for solutes. To simulate non-calibrated flow and conservative transport, we assumed that Pile 2 and Pile 5 were exposed to the same precipitation rates and climatic conditions. The top of the column of material above Pile 5B receiving precipitation was composed of the intrusive material, classified as "Class A" waste rock, (Blackmore et al., 2018), as Pile 2. As such, recharge rates, flow and conservative transport parameters for our model were considered the same as those for Class "A" of Pile 5 (Table 1). Initial dissolved concentrations of Cl were estimated from maximum concentrations observed from the BTC (100 mgL^{-1}). From Blackmore et al. (2018), we retained the same mass-transfer coefficient of $\omega = 5.21 \times 10^{-9}$ s^{-1} and the total porosity of $\theta = 0.24$, split into a mobile porosity $\theta_m = 0.06$ and an immobile porosity

Table 1
Physical parameters used in the model analyses.

Parameter	Value	Unit
Saturated hydraulic conductivity K_z	5×10^{-4}	ms^{-1}
Residual saturation S_r	5×10^{-2}	–
Van Genuchten α (mobile region)	1.8	m^{-1}
Van Genuchten n (mobile region)	1.27	–
Van Genuchten l (mobile region)	5×10^{-1}	–
Free diffusion coefficient in water D_w	2.38×10^{-9}	m^2s^{-1}
Free diffusion coefficient in air D_g	2.07×10^{-5}	m^2s^{-1}
Longitudinal dispersivity α_L (mobile region)	3×10^{-1}	m
Total porosity θ	2.4×10^{-1}	–
Mobile porosity θ_m	8×10^{-2}	–
Immobile porosity θ_{im}	1.6×10^{-1}	–
Mass transfer coefficient ω	5.2×10^{-9}	s^{-1}

θ_{im}=0.18.

2.3.2. Dual-domain multicomponent reactive transport

The geochemical reactions incorporated in the DDMRTM model were selected according to the *adagio* 'as simple as possible, but as complicated as necessary' and include a purposely limited set of reactions to maximize model transparency. Simplifications and assumptions made for the geochemical model include:

- Sulfate and acidity are generated exclusively by oxidation of pyrite and molybdenite.
- Calcite is the only mineral buffering the drainage acidity. Other carbonates and silicates known to occur at Antamina were not part of the geochemical reaction network, as their buffering capacity was small compared to that provided by calcite (Vriens et al., 2019a).
- Gypsum, powellite and ferrihydrite are the only secondary mineral phases considered, providing the dominant solubility controls for Ca, MoO_4^{2-}, SO_4^{2-} and Fe^{3+}.
- Powellite was used as the sole secondary mineral phase containing Mo. (Conlan et al., 2012; Skierszkan et al., 2016; Hirsche et al., 2017; Vriens et al., 2019c). Given the low amount of Pb in Pile 2, wulfenite [$PbMoO_4$], another potential Mo-bearing secondary mineral observed in other Antamina waste rock (Conlan et al., 2012), was expected to be negligible as a Mo-sink above SL2B.
- Pore-gas concentrations, measured in Pile 2 using in-situ instrumentation (Lorca et al., 2016; Vriens et al., 2019b), showed near atmospheric levels for O2 and elevated CO2, and in the model were fixed to O2(g) = 21% (*v*/v) and CO2(g) = 0.1% (v/v)

The main geochemical parameters used in the DDRMTM analysis are listed in Table 2. This table also reports the initial volumetric fractions (ψ) of the reactive minerals used in the simulations, their stoichiometries and equilibrium constants (log K), as well as the aqueous concentrations of the components characterizing the recharging and initial background pore waters. Table 2 also includes the composition of the infiltrating precipitation and the initial porewater for the reactive transport modeling.

Table 2
(a) Minerals, corresponding formulae, thermodynamic equilibrium constants (log K) and initial volume fractions used in the modeling analyses. The specific values adopted in the various sensitivity analyses are reported in the text. (b) Aqueous components and their concentrations in the recharging and initial background pore water. All information is applicable to mobile and immobile domains.

(a) Mineral [formula]	log K	vol. frac.
Calcite [$CaCO_3 \rightleftharpoons Ca^{2+} + CO_3^{2-}$]	8.48	10^{-2}
Ferrihydrite [$Fe(OH)_3 + 3\,H^+ \rightleftharpoons Fe^{3+} + H_2O$]	4.89	–
Gypsum [$CaSO_4 \rightleftharpoons Ca^{2+} + SO_4^{2-} + 2$ H2O]	4.58	–
Molybdenite [$MoS_2 + 4.5O_{2(aq)} + 3H_2O \rightleftharpoons MoO_4^{2-} + 2SO_4^{2-} + 6H^+$]	*irreversible dissolution, log K not defined*	3.3×10^{-6}
Powellite [$CaMoO_4 \rightleftharpoons Ca^{2+} + MoO_4^{2-}$]	7.95	–
Pyrite [$FeS_2 + 3.5O_{2(aq)} + H_2O \rightleftharpoons Fe^{2+} + 2SO_4^{2-} + 2H^+$]	61.49	5×10^{-2}
(b) Aqueous components	Input/background concentration	units
Ca^{2+}	3.8×10^{-4}	mol L^{-1}
Cl^-	3.8×10^{-4}	mol L^{-1}
CO_3^{2-}	Equilibrium with atmospheric $CO_{2(g)}$	mol L^{-1}
Fe^{2+}	6.3×10^{-6}	mol L^{-1}
Fe^{3+}	4.5×10^{-14}	mol L^{-1}
MoO_4^{2-}	2.5×10^{-10}	mol L^{-1}
$O_{2(aq)}$	Equilibrium with atmospheric $O_{2(g)}$	mol L^{-1}
SO_4^{2-}	10^{-5}	mol L^{-1}
pH	5.65	–

MIN3PDUAL utilizes a kinetic formulation for reaction rates (R_x) of reversible, surface-controlled dissolution-precipitation reactions (Mayer et al., 2002). A precipitation or dissolution rate R_x was defined for each mineral x as:

$$R_x = k_x \left[1 - \frac{IAP_x}{K_x}\right] \tag{6}$$

where k_x is a zero-order kinetic-rate coefficient and IAP_x the ion activity product. Rate coefficients were set to yield quasi-equilibrium conditions for calcite, gypsum and ferrihydrite. A sensitivity analysis (not shown) suggested that our models were insensitive to rate coefficients used to simulate powellite precipitation, which is kinetically limited (Conlan et al., 2012; Skierszkan et al., 2019a). Therefore, we also imposed quasi-equilibrium conditions for powellite. Mineral-specific thermodynamic equilibrium constants K_x were based on the MINTEQA2 database, version 4 (Allison et al., 1998).

We modeled pyrite and molybdenite oxidation as zero-order irreversible processes, in the absence of supporting data that could justify more complex modeling formulations for sulfide weathering (for instance, a shrinking-core model). This choice was also made to limit the number of model unknowns and potential complexity of the model interpretation. The zero-order approach is further justified by mass-balance analyses of the drainage from Pile 2 and its bulk waste-rock Fe-content (Vriens et al., 2019a), which suggest that Fe-depletion in Pile 2 was <10% over 10 years. After initial tests, we fixed the pyrite rate coefficient at $k_{FeS2} = 5 \times 10^{-10}$ mol L^{-1} s^{-1}, which allows the simulation to match the observed release of SO_4^{2-} (and indirectly Ca through the precipitation of gypsum) and the drainage pH, which does not drop substantially. This value for k_{FeS2} is in line with other works on sulfide-rich WRPs using similar modeling approaches (Javadi, 2019). For molybdenite, the value of k_{MoS2} was more difficult to estimate a priori, and it remains poorly constrained in the literature (Johnson et al., 2019). Thus, it was instead treated as a fitting parameter. The best-fitting parameter was obtained using an iterative procedure that minimizes the root mean square error (RMSE) between observed and simulated values.

Adsorption onto mineral surfaces is an additional process attenuating Mo drainage concentrations. Adsorption can become the dominant attenuating process in oxic and sub-oxic waste-rock environments (Skierszkan et al., 2019b). Nonlinear Mo sorption, in which a greater proportion adsorbs at low concentrations, has been previously observed and inferred to explain Mo tailing behavior (Stollenwerk, 1995). Under oxic conditions at pH < 6, molybdate may be strongly adsorbed through inner-sphere complexation with Fe-(oxyhydr)oxides. Under circumneutral pH, however, molybdate sorption involves weaker outer-sphere complexation that can lead to enhanced Mo mobility in circumneutral to slightly alkaline drainage pH, as observed in Pile 2B (Skierszkan et al., 2016; Vriens et al., 2019b).

Adsorption of Mo to prototypical hydrous ferrous oxides (HFOs) and select other Fe-minerals (ferrihydrite, hematite and goethite) has been studied previously (Goldberg et al., 2009; Arai, 2010; Kashiwabara et al., 2011; Gustafsson and Tiberg, 2015). Adsorption of Mo on HFOs was implemented in the DDMRTM as a reversible equilibrium-controlled term, aggregating the variety of experimentally detected Fe-(oxyhydr)oxide phases in "Class A" Antamina waste rock (Vriens et al., 2019c, 2019a) under a single idealized HFO phase (" ≡ FeOH"). A non-electrostatic surface complexation model (SCM) was adopted. The MINTEQA2 database contains pH-dependent sorption surfaces, forming from the binding between cations and anions (including Mo species) onto strong (" ≡ FeOH(s)") and weak (" ≡ FeOH(w)") surface sites (Dzombak and Morel, 1990). A list of the considered surface species, their formulae and log K values is provided in Table 3.

Table 3
Surface complexation reactions used in the simulations, with corresponding formula and log K.

Sorption surface formula	Log K
Strong surfaces binding with "≡FeOH(s)"	
$\equiv FeOH_2^+(s) \rightleftharpoons H^+ + \equiv FeOH(s)$	7.29
$\equiv FeO^-(s) + H^+ \rightleftharpoons \equiv FeOH(s)$	8.93
$\equiv FeOCa^-(s) + H^+ \rightleftharpoons Ca^{2+} + \equiv FeOH(s)$	4.97
$\equiv FeOFe^-(s) + H^+ \rightleftharpoons Fe^{2+} + \equiv FeOH(s)$	0.7
Weak surfaces binding with "≡FeOH(w)"	
$\equiv FeOH_2^+(w) \rightleftharpoons H^+ + \equiv FeOH(w)$	7.29
$\equiv FeO^-(w) + H^+ \rightleftharpoons \equiv FeOH(w)$	8.93
$\equiv FeMoO_4(w) + H_2O \rightleftharpoons MoO_4^{2-} + 2H^+ + \equiv FeOH(w)$	9.5
$\equiv FeOHMoO_4^{3-}(w) + H^+ \rightleftharpoons MoO_4^{2-} + \equiv FeOH(w)$	2.4
$\equiv FeOHSO_4^-(w) + H_2O \rightleftharpoons SO_4^{2-} + \equiv FeOH(w) + H^+$	7.78
$\equiv FeOHSO_4^{2-}(w) \rightleftharpoons SO_4^{2-} + \equiv FeOH(w)$	0.79
$\equiv FeCO_3^-(w) + H_2O \rightleftharpoons CO_3^{2-} + \equiv FeOH(w) + H^+$	12.56
$\equiv FeHCO_3(w) + H_2O \rightleftharpoons CO_3^{2-} + \equiv FeOH(w) + 2H^+$	20.62

The SCM depends on the total concentration of the surfaces where Mo can adsorb, C_{surf} (mol L^{-1}), expressed in MIN3P as:

$$C_{surf} = 10^{-9} A_v \sigma_s \Lambda \quad (7)$$

where A_v is the Avogadro constant (mol/sites), σ_s is the density of reactive HFO sites (sites nm^{-2}) and Λ (m^2L^{-1}) is obtained as

$$\Lambda = S_s M_s \quad (8)$$

where M_s is the mass of the sites (g L^{-1}) and S_s is the specific surface area of the HFO (m^2 g^{-1}). For σ_{HFO}, we considered that HFO contains 50 μmol m^{-2} of sorption sites(Dzombak and Morel, 1990), resulting in $\sigma_s \approx 6$ sites nm^{-2}, consistent with the previous analyses involving the adopted SCM model (Davis and Kent, 1990; Appelo and Postma, 2005; Demers et al., 2013). An estimation of M_s based on our mineralogical data (Vriens et al., 2019a) shows that the abundance of HFO, assumed as aggregate for all secondary Fe-(oxyhydr)oxides was 0.1 wt-% at the beginning of the simulations. Assuming that this amount is an average value that remains constant with time (in reality, HFO will grow and undergo phase changes as weathering proceeds), this corresponds to a mass of HFOs above SL2B of M_s = 8.8 gL^{-1}, adopting the total porous volume of the projected waste rock and its mean density above sub-lysimeter Pile 2 (Vriens et al., 2019b). This value is of the same order of magnitude, but about 4.5× lower, for instance, than the adopted value by Demers et al. (2013) for another, slightly more fine-grained waste-rock pile (M_s=40 gL^{-1}).

The estimation of S_s was more uncertain, because we lacked specific surface area measured on waste-rock particles (e.g., BET) and because the heterogeneity of waste rock renders it complicated to provide average (upscaled) values for the broad range of materials in this pile. A first-cut estimation of S_s was obtained by assuming that all waste-rock particles exhibited a uniform spherical geometry, that density was uniform across the entire particle-size distribution, and that mineral phases were homogeneously distributed over the different size fractions. This way, we obtained a range of S_s=0.2–3 m^2g^{-1} HFOs, which is in line with the results from other waste-rock studies, e.g. S_s=0.8 m^2g^{-1} HFOs reported by Demers et al. (2013). Due to the adopted simplifications, however, the range of S_s remains uncertain. The fact that waste rock is a coarse material explains at least in part that the surface area is approximately two orders of magnitude smaller than typical values reported in the literature for sorption on HFO minerals (Appelo and Postma, 2005). Also, not all waste-rock minerals contain reactive iron. As such, we assumed a base-case value of S_s=1 m^2g^{-1} HFOs (an intermediate value representative of the field-based estimation) and performed a sensitivity around this value.

3. Results: analysis and discussion

3.1. Analysis of the observed BTCs

The shape of the double-log plots of Cl and Mo drainage concentrations over time (Fig. 4, red symbols) are diagnostic to evaluate whether upscaled transport simulation using DDM formulations is a reasonable choice for the selected case study. The observed BTCs of Cl and Mo show that conservative Cl behaves distinctly from reactive Mo in Pile 2B. For Cl, the BTC concentrations are initially high and gradually trend towards lower concentrations through time, illustrative of the conservative nature of Cl. It can further be observed that the double-log BTC for Cl displays patterns indicative of mobile-immobile transport. Namely, the shape of the double-log BTC of Cl is strongly asymmetric and its tailing (i.e. the post-peak part of the BTC) can be described by a power-law function with slope

$$C \propto t^{-\beta} \quad (9)$$

where C is concentration, t is time and β is the power-law exponent. For Cl, we find that the tails scale close to β=3/2, the characteristic slope of BTC tailings determined analytically for non-equilibrium matrix diffusion models in dual-porosity systems (Hadermann and Heer, 1996), which are conceptually and mathematically similar to a DDM model. Although much longer records would be needed to properly identify a power-law scaling of the BTCs compared to other heavily tailed statistical models (Pedretti and Bianchi, 2018), the data suggests that a dual-domain transport formulation is a reasonable choice to describe the behavior of conservative tracers like Cl in the studied WRP.

Compared to Cl, the BTC of Mo (Fig. 4, blue symbols) shows a relatively elongated shape with an initially delayed mobilization as well as a gradual reduction of leachate concentrations over the course of several years. Considering that no geochemical processes inhibited the mobility of Cl in these simulations, we contrast Cl as a reference conservative tracer and Mo as a reactive tracer. The reactive nature of Mo can be phenomenologically appreciated from its BTC when plotted in double-log normalization (Fig. 4, blue symbols). Firstly, the rising part of the BTC of Mo is delayed compared to that of Cl, indicating that Mo release is slower than conservative transport. This is consistent with the kinetic release of Mo by the weathering of Mo-bearing sulfides, contrasting the quicker release of Cl that is associated to a "first flush" of soluble Cl-

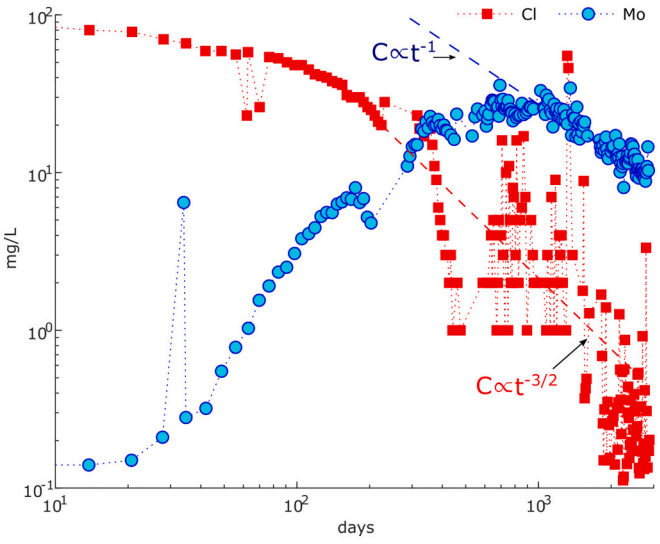

Fig. 4. Observed drainage chemistry record for Mo and Cl in SL2B plotted on logarithmic concentration- and time scales, emphasizing the power-law-like scaling of both Mo and Cl breakthrough curve tails, with different characteristic exponents.

bearing salts. In addition, the BTC tail for Mo scales close to $\beta = 1$, i.e. a smaller exponent than that for Cl, suggesting a higher persistence of Mo in the waste-rock matrix compared to Cl, and consistent with an internal release limitation and/or attenuation process beyond purely conservative mass transport.

3.2. Flow and conservative transport modeling

A comparison between forward-simulated cumulative flow and Cl exfiltrating at Pile 2B and the observed values is shown in Fig. 5. We contrasted the DDM simulations against single-domain simulations, i.e. the results from the use of a classic one-dimensional single-domain advection dispersion equation (ADE), obtained by setting $\omega = 0$. The test was performed by setting the concentration of Cl in the water resident in the pile at the start of the simulation to 100 mgL^{-1}.

Considering that the DDM model parameters were not calibrated but obtained directly from "Class A" materials for Pile 5B, both flow (top plot) and conservative Cl records (middle and bottom plots) were reasonably well reproduced. Both the single-domain and DDM model simulations quantitatively agree with measured values in cumulative drainage from Pile 2B (flow is the same in both ADE-based and DDM-based models). In arithmetic scales, both the initial (maximum) concentrations and the decrease in concentration ($C \rightarrow 0$) are correctly captured by both models.

However, the use of linear scales obscures the performance of the transport models at lower concentrations, i.e., the BTC tails, which are key for identifying mass transfer between the zones of different mobility. More importantly, the BTC tails are key features to obtain WRP model parameters that can describe the long-term behavior of solute transport. It is important that models used to assist decision makers for prediction of post-closure contaminant transport from WRPs properly reproduce the BTC tails and the evolution of the contaminants at timescales far beyond those characterizing the initial weathering process. When plotted on a logarithmic concentration scale (bottom plot of Fig. 5), the differences between the ADE and the DDM outputs become more noticeable. On the tails, the dual-domain model sustains Cl concentrations in line with those measured in the field, whereas the single-porosity model yields a too rapid decrease in Cl concentrations.

The fact that the DDM provides a superior fit of the experimental BTCs compared to the single-domain ADE model corroborates the findings by Blackmore et al (Blackmore et al., 2018), who obtained a superior fit for the BTC of Cl from Pile 5B with the DDM model compared to a single-domain model. Better agreement with dual-porosity over single-porosity formulations was also obtained in several other analyses from systems embedding different flow geometries (Sánchez-Vila and Carrera, 2004; Molinari et al., 2015; Sharma et al., 2015), owing to the fact that the mass transfer between mobile and immobile domains effectively accounts for the small-scale heterogeneities that cannot be reproduced using a 1-D ADE model. Since the results of the conservative transport modeling indicate that a single-domain (ADE) formulation

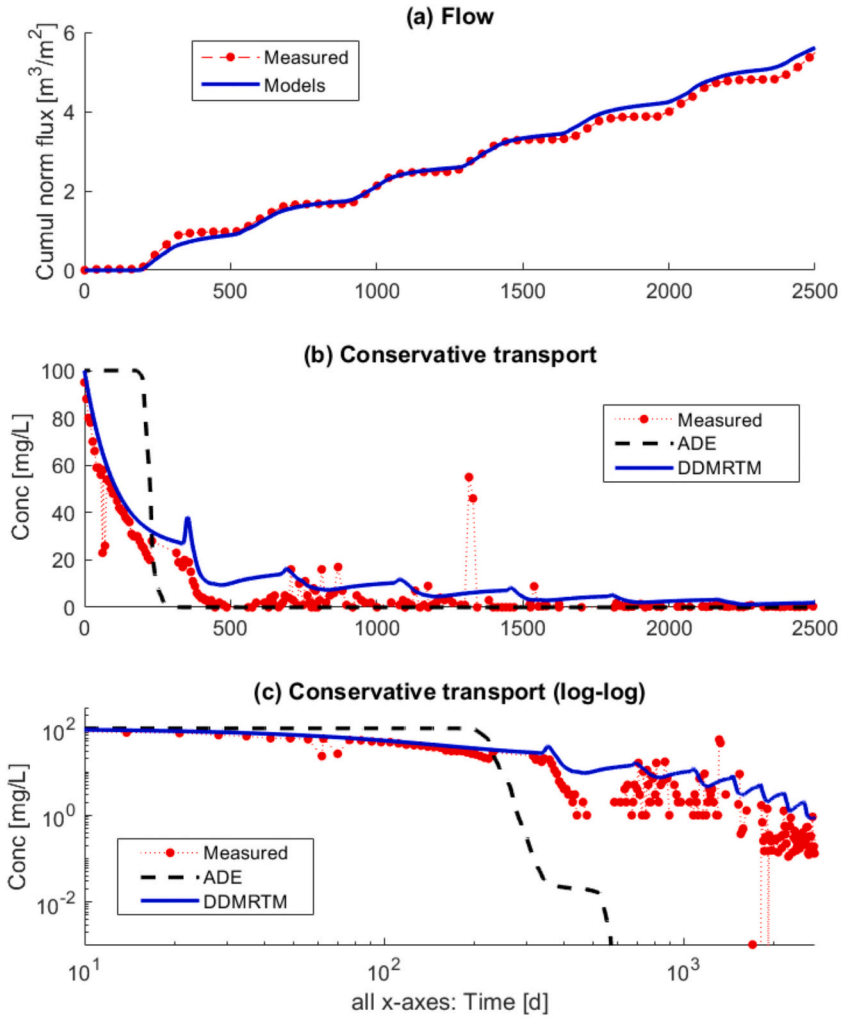

Fig. 5. Observed and simulated (a) cumulative flow rates observed at Pile 2B (same result for both the ADE and the DDMRMT models), and Cl BTCs plotted on linear (b) and double-log (c) scales.

does not well describe solute transport in SL2B, the focus of the remaining work is to reproduce drainage dynamics of the reactive solutes using dual-domain formulations only. Finally, the conservative transport simulations indicate that the DDM model for Pile 2B was able to reproduce field observations using parameters calibrated towards a specific portion of Pile 5B, which had a similar lithology as Pile 2B (i.e., intrusive rocks). Therefore, DDM transport parameters determined for materials with similar grain-sizes appear to be transferable to other systems, although further confirmation across grain-size ranges is required.

3.3. Dual-domain multicomponent reactive transport modeling

The result of the DDMRTM simulation embedding the calibrated, best-fitting $k_{MoS2} = 4 \times 10^{-13}$ mol L^{-1} s^{-1} (resulting in RMSE = 0.14) are shown in Fig. 6a and Fig. 6b, which compare the Mo breakthrough curves and the cumulative Mo mass against measured data. Fig. 6c provides the Ca BTC, the drainage pH and the SO_4 BTC from Pile 2B, respectively.

The DDMRTM model captures the recorded drainage pH and SO_4 concentrations accurately, while only marginally overpredicting Ca concentrations in SL2B drainage. Molybdenum BTCs (Fig. 6a) and the corresponding cumulative values (Fig. 6b) are reproduced equally well, capturing the buildup segment of the observed BTC. The model is able to capture the early-time arrival of the Mo BTC at the sub-lysimeter, the maximum observed Mo concentrations and the BTC tails (i.e., >1500 days). Overall, the model appears to properly reproduce Mo concentrations, in agreement with the Cl BTC tail that the dual-domain model could quantitatively reproduce (Fig. 5). The model also satisfactorily captures the cumulative amount of Mo released from SL2B. The relatively stable Ca and SO_4 drainage concentrations are strongly tied to the solubility limit of secondary gypsum, as has been previously experimentally observed (Vriens et al., 2019a).

We thus conclude that a DDMRTM is appropriate to reproduce the observed drainage record. It is particularly relevant that the model works well using just one fitting parameter, i.e. the rate constant for molybdenite oxidation (k_{MoS2}). A sensitivity analysis performed to evaluate the uncertainty around this parameter suggested (Fig. 7) that a small variation of k_{MoS2} causes large variations in the modeled Mo BTC resulting in substantial discrepancies in the cumulative Mo from the reference best-fit simulation. This is true for both an increase (green lines with square markers) and a decrease (light blue lines with crosses) in k_{MoS2}, indicating that the parameter is identifiable (well constrained) by the Mo concentration data and is essential to accurately reproduce

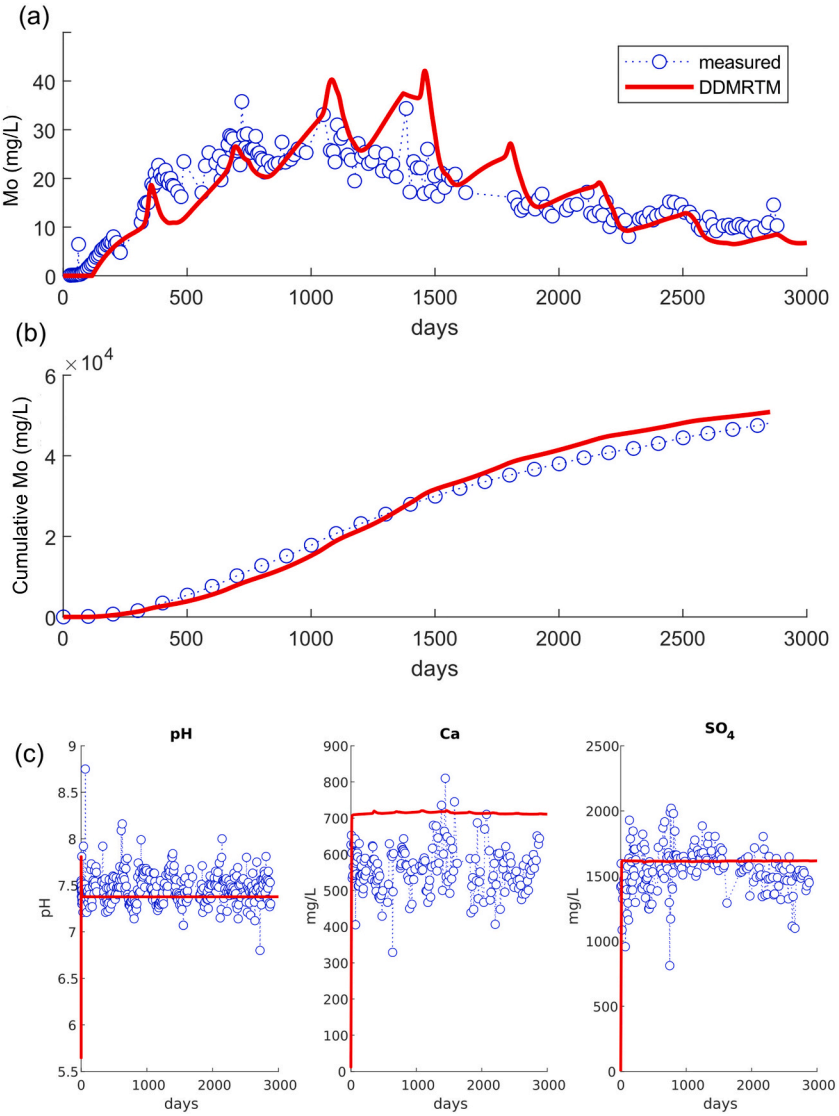

Fig. 6. Observed and simulated aqueous concentrations of molybdenum, calcium, sulfate and pH and in SL2B drainage using the best-fit dual-domain multicomponent reactive transport model (DDMRTM).

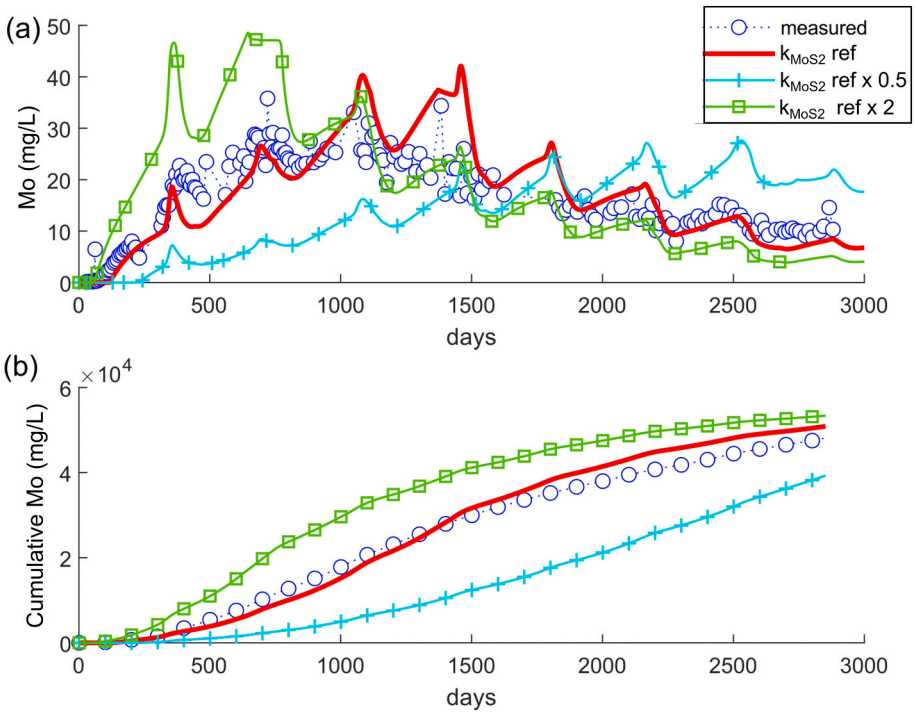

Fig. 7. Sensitivity analysis around the rate constant for molybdenite oxidation (k_{MoS2}). (a) Simulated BTCs of Mo as SL2B using different values of k_{MoS2}. (b) cumulative concentrations. Each curve refers to a model embedding a parameter obtained multiplying the reference value (ref) ($k_{MoS2} = 4 \times 10^{-13}$mol L^{-1} s^{-1}) by the value reported in the legend.

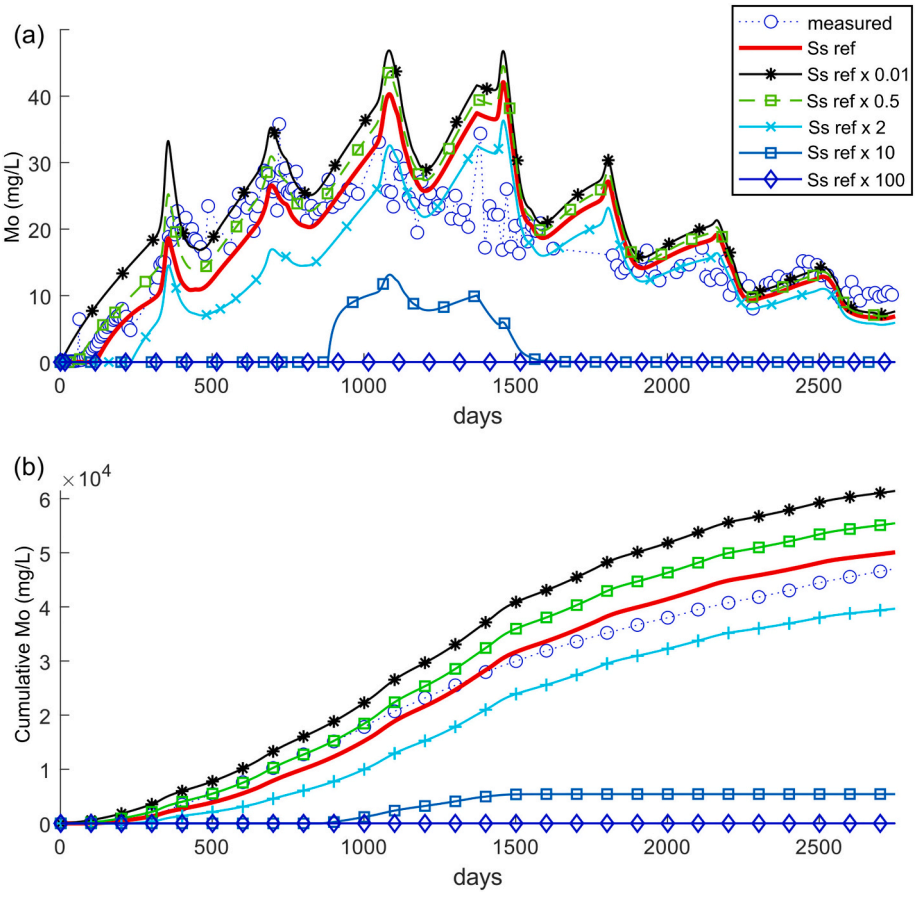

Fig. 8. Sensitivity analysis around the specific surface area of the HFO (S_s). (a) Simulated BTCs of Mo as SL2B using different values of S_s. (b) cumulative concentrations. Each curve refers to a model embedding a parameter obtained multiplying the reference value (ref) (S_s=1 m^2g^{-1}) by the value reported in the legend.

the pile's drainage.

A sensitivity analysis was also conducted around another uncertain parameter, the specific surface area of the HFO (S_s), while keeping the $k_{MoS2} = 4x10^{-13}$ mol L^{-1} s^{-1}. The results (.

Fig. 8) suggested that the model was relatively insensitive to a decrease in S_s, as comparable results are obtained in simulations with a multiplicative factor up to 0.01× (i.e., to S_s=0.01 m^2g^{-1}). Instead, simulations with larger S_s reveal the opposite behavior. Multiplicative factors 10× (S_s=10 m^2g^{-1}) and 100× (S_s=100 m^2g^{-1}) produce strongly decreasing, and ultimately negligible Mo concentrations, respectively. These results suggest that the presence of additional sorption sites would strongly attenuate the mobility of Mo, but also that HFO (and other minerals) may currently be controlling the net-adsorption of Mo: because there appear to be limited available sorption sites, Mo exhibits relatively elevated mobility in the studied pile.

No significant variations in Ca, SO_4 and pH were observed in the sensitivity analyses, which instead remained at levels similar to those of the best-fit model (data not shown). Finally, simulations also revealed that competition for sorption sites by other anions did not influence the long-term Mo record (results not reported). The drainage from SL2B exhibited concentrations of potentially competing oxyanions (phosphate, arsenate, tungstate, or chromate) (Smedley and Kinniburgh, 2017) that were either below detection limits or at least an order-of-magnitude lower than Mo concentrations (Vriens et al., 2019b). The inferred lack of competition for sorption sites is consistent with previous studies that found that tungstate and phosphate appear to be the strongest competitors of Mo for the adsorption sites of goethite, whereas only minor competitive effects were observed in the case of silicate and sulfate (Xu et al., 2009).

4. Conclusion

Upscaled (or "effective") models are appealing for modeling reactive transport in complex systems due to a reduced computational burden compared to multidimensional reactive transport models. However, a drawback of effective models is that linking physical and mathematical DDM parameters is highly difficult. Consequently, in many practical applications, upscaled model parameters are treated as empirical parameters that are fitted to site-specific observations such as solute BTCs from tracer tests. This fitting casts legitimate doubts regarding the predictive ability of upscaling models and their calibrated parameters.

This work presented reactive transport simulations with single- and dual-domain multicomponent reactive-transport models (DDMRTMs) and corresponding parameter sensitivity analyses for the prediction of conservative and reactive solute transport through a mine waste-rock pile. Our work is one of the first ever presented application of a DDMRTM model for upscaling purposes on waste-rock drainage.

We found that the dual-domain formulation outperformed its single-domain counterpart in the reproduction of conservative (Cl) solute trends, in line with previous studies (Blackmore et al., 2018). Experimentally pre-calibrated parameters of the dual-domain model (e.g., van Genuchten parameters, particle sizes, mineral fractions, kinetic mass transfer coefficients) appeared extrapolatable across similar-scale experiments with comparable material types. In this sense, our results prove that linking physical and mathematical dual-domain parameters is not impossible.

The DDMRTM model successfully simulated long-term Mo drainage chemistry dynamics. The ultimate best-fit model and parameters were consistent with the current mechanistic understanding of Mo waste-rock geochemistry. The great majority of model parameters were established by experimental evidence or literature values. A critical fitting parameter remains the kinetic rate coefficient for molybdenite oxidation, k_{MoS2}, which the model is very sensitive to. An increase in k_{MoS2} could be balanced out by increasing the surface complexation (the sink term).

We thus conclude that the DDMRTM model works well for reproducing BTCs of drainage from reactive waste-rock piles. As such, we recommend the DDMRTM approach going forward for upscaling waste-rock drainage. A proper characterization of source and sink terms in waste rock will provide better constraints for DDMRTM predictions.

Research data

All data used in this work are available through previously published work (Vriens et al., 2019a).

CRediT author statemetn

Daniele Pedretti: Data curation, Writing- Original draft preparation, Conceptualization, Methodology, Software, Visualization, Investigation, Reviewing.

Bas Vriens: Data curation, Writing- Original draft preparation, Conceptualization, Methodology, Reviewing.

Elliot E. Skierszkan: Data curation, Writing- Original draft preparation, Investigation.

Petra Baják Original draft preparation.

K. Ulrich. Mayer Writing- Original draft preparation and Editing, Supervision, Project coordinator.

Roger. D. Beckie Writing- Original draft preparation and Reviewing, Supervision, Project coordinator.

Declaration of Competing Interest

The authors declare that they have no known competing financial interests or personal relationships that could have appeared to influence the work reported in this paper.

Acknowledgments

We acknowledge the valuable comments by the two anonymous Reviewers who revised the original manuscript. We gratefully acknowledge technical and logistical support from the Antamina mine with the construction, monitoring, and sampling of the experimental piles. Financial support was provided by Compañia Minera Antamina S. A., the Natural Science and Engineering Research Council of Canada (NSERC, grant CRDPJ334909-2005), and Teck Metals Limited's Applied Research and Technology Group. (b) The results here presented have been developed in the frame of the MIUR Project "Dipartimenti di Eccellenza 2017—Le Geoscienze per la società: risorse e loro evoluzione". (c) This research is also part of a project that has received funding from the European Union's Horizon 2020 research and innovation program under grant agreement No 810980.

References

Allison, J.D., Brown, D.S., Novo-Gradac, K.J., 1998. MINTEQA2/PRODEFA2, A geochemical assessment model for environmental systems: User manual supplement for version 4.0. In: Environ. Res. Lab., Office of Res, and Dev. USEPA, Athens, GA. Available online. https://www.epa.gov/sites/production/files/documents/SUPPLE1.PDF.

Amos, R.T., Blowes, D.W., Bailey, B.L., Sego, D.C., Smith, L., Ritchie, A.I.M., 2015. Waste-rock hydrogeology and geochemistry. Appl. Geochem. 57, 140–156. https://doi.org/10.1016/j.apgeochem.2014.06.020.

Appelo, C.A.J., Postma, D., 2005. Geochemistry, Groundwater and Pollution. Geochemistry, Groundwater and Pollution. A.A. Balkema Publishers (Ed.2).

Arai, Y., 2010. X-ray absorption spectroscopic investigation of molybdenum multinuclear sorption mechanism at the goethite−water interface. Environ. Sci. Technol. 44 (22), 8491–8496. https://doi.org/10.1021/es101270g.

Asher, M.J., Croke, B.F.W., Jakeman, A.J., Peeters, L.J.M., 2015. A review of surrogate models and their application to groundwater modeling. Water Resour. Res. 51 (8), 5957–5973.

Blackmore, S., Pedretti, D., Mayer, K.U., Smith, L., Beckie, R.D., 2018. Evaluation of single- and dual-porosity models for reproducing the release of external and internal tracers from heterogeneous waste-rock piles. J. Contam. Hydrol. 214, 65–74. https://doi.org/10.1016/j.jconhyd.2018.05.007.

Blowes, D.W., Ptacek, C.J., Jambor, J.L., Weisener, C.G., 2003. The geochemistry of acid mine drainage. Treat Geochem. Elsevier 149–204.

Cheng, L., 2006. Dual Porosity Reactive Transport Modeling. PhD Thesis. The University of Sheffield, Sheffield, UK.
Cheng, L., Mayer, K.U., Oswald, S., Lerner, D.N., 2004. Dual-Porosity Multi-Component Reactive Transport Model MIN3PDUAL and Application. European Geosciences Union 1st General Assembly, Nice, France.
Conlan, M.J.W., Mayer, K.U., Blaskovich, R., Beckie, R.D., 2012. Solubility controls for molybdenum in neutral rock drainage. Geochem. Explor. Environ. Anal. 12 (1), 21–32. https://doi.org/10.1144/1467-7873/10-RA-043.
Davis, J.A., Kent, D.B., 1990. Surface complexation modeling in aqueous geochemistry. Rev. Mineral. Mineral. Soc. Am. 23, 177–259.
Demers, I., Molson, J., Bussière, B., Laflamme, D., 2013. Numerical modeling of contaminated neutral drainage from a waste-rock field test cell. Appl. Geochem. 33, 346–356. https://doi.org/10.1016/j.apgeochem.2013.02.025.
Donado, L.D., Sanchez-Vila, X., Dentz, M., Carrera, J., Bolster, D., 2009. Multicomponent reactive transport in multicontinuum media. Water Resour. Res. 45 (11).
Dzombak, D.A., Morel, F.M., 1990. Surface Complexation Modeling: Hydrous Ferric Oxide. John Wiley & Sons, New York, NY, USA.
Fala, O., Molson, J., Aubertin, M., Dawood, I., Bussière, B., Chapuis, R.P., 2013. A numerical modelling approach to assess long-term unsaturated flow and geochemical transport in a waste rock pile. Int. J. Min. Reclam. Environ. 27 (1), 38–55. https://doi.org/10.1080/17480930.2011.644473.
Fiori, A., Zarlenga, A., Gotovac, H., Jankovic, I., Volpi, E., Cvetkovic, V., Dagan, G., 2015. Advective transport in heterogeneous aquifers: are proxy models predictive? Water Resour. Res. 51 (12), 9577–9594. https://doi.org/10.1002/2015WR017118.
Gerke, H.H., Molson, J.W., Frind, E.O., 1998. Modelling the effect of chemical heterogeneity on acidification and solute leaching in overburden mine spoils. J. Hydrol. 209 (1–4), 166–185.
Goldberg, T., Archer, C., Vance, D., Poulton, S.W., 2009. Mo isotope fractionation during adsorption to Fe (oxyhydr)oxides. Geochim. Cosmochim. Acta 73 (21), 6502–6516. https://doi.org/10.1016/j.gca.2009.08.004.
Gustafsson, J.P., Tiberg, C., 2015. Molybdenum binding to soil constituents in acid soils: an XAS and modelling study. Chem. Geol. 417, 279–288. https://doi.org/10.1016/j.chemgeo.2015.10.016.
Hadermann, J., Heer, W., 1996. The Grimsel (Switzerland) migration experiment: integrating field experiments, laboratory investigations and modelling. J. Contam. Hydrol. 21 (1–4), 87–100. https://doi.org/10.1016/0169-7722(95)00035-6.
Hirsche, D.T., Blaskovich, R., Mayer, K.U., Beckie, R.D., 2017. A study of Zn and Mo attenuation by waste-rock mixing in neutral mine drainage using mixed-material field barrels and humidity cells. Appl. Geochem. 84 (Supplement C), 114–125. https://doi.org/10.1016/j.apgeochem.2017.06.005.
INAP-GARD, 2014. GARD (Global Acid Rock Drainage) Guide the International Network for Acid Prevention (INAP). URL. http://www.gardguide.com/.
Javadi, M., 2019. Reactive Transport Modeling of Unsaturated Hydrology and Geochemistry of Neutral and Acid Rock Drainage in Highly Heterogeneous Mine Waste Rock at the Antamina Mine. University of British Columbia, Peru.
Johnson, A.C., Romaniello, S.J., Reinhard, C.T., Gregory, D.D., Garcia-Robledo, E., Revsbech, N.P., Canfield, D.E., Lyons, T.W., Anbar, A.D., 2019. Experimental determination of pyrite and molybdenite oxidation kinetics at nanomolar oxygen concentrations. Geochim. Cosmochim. Acta 249, 160–172. https://doi.org/10.1016/j.gca.2019.01.022.
Kashiwabara, T., Takahashi, Y., Tanimizu, M., Usui, A., 2011. Molecular-scale mechanisms of distribution and isotopic fractionation of molybdenum between seawater and ferromanganese oxides. Geochim. Cosmochim. Acta 75 (19), 5762–5784. https://doi.org/10.1016/j.gca.2011.07.022.
Lahmira, B., Lefebvre, R., Aubertin, M., Bussière, B., 2016. Effect of heterogeneity and anisotropy related to the construction method on transfer processes in waste rock piles. J. Contam. Hydrol. 184 (Supplement C), 35–49. https://doi.org/10.1016/j.jconhyd.2015.12.002.
Lorca, M.E., Mayer, K.U., Pedretti, D., Smith, L., Beckie, R.D., 2016. Spatial and temporal fluctuations of pore-gas composition in sulfidic mine waste rock. Vadose Zone J. 15 (10) https://doi.org/10.2136/vzj2016.05.0039, 0.
Mayer, K.U., Frind, E.O., Blowes, D.W., 2002. Multicomponent reactive transport modeling in variably saturated porous media using a generalized formulation for kinetically controlled reactions: reactive transport modeling in variably saturated media. Water Resour. Res. 38 (9) https://doi.org/10.1029/2001WR000862, 13-1-13–21.
Molinari, A., Pedretti, D., Fallico, C., 2015. Analysis of convergent flow tracer tests in a heterogeneous sandy box with connected gravel channels. Water Resour. Res. 51 (7), 5640–5657. https://doi.org/10.1002/2014WR016216.
Molson, J., Aubertin, M., Bussière, B., 2012. Reactive transport modelling of acid mine drainage within discretely fractured porous media: plume evolution from a surface source zone. Environ. Model. Softw. 38, 259–270. https://doi.org/10.1016/j.envsoft.2012.06.010.
Muniruzzaman, M., Pedretti, D., 2020. Mechanistic models supporting uncertainty quantification of water quality predictions in heterogeneous mining waste rocks: a review. Stoch. Env. Res. Risk A. https://doi.org/10.1007/s00477-020-01884-z.
Neuman, S.P., Tartakovsky, D.M., 2009. Perspective on theories of non-Fickian trasport in heterogeneous media. Adv. Water Resour. 32, 670–680.
Nichol, C., Smith, L., Beckie, R., 2005. Field-scale experiments of unsaturated flow and solute transport in a heterogeneous porous medium. Water Resour. Res. 41 (5), W05018. https://doi.org/10.1029/2004WR003035.
Pedretti, D., Bianchi, M., 2018. Reproducing tailing in breakthrough curves: are statistical models equally representative and predictive? Adv. Water Resour. 113, 236–248. https://doi.org/10.1016/j.advwatres.2018.01.023.
Pedretti, D., Fernàndez-Garcia, D., Sanchez-Vila, X., Bolster, D., Benson, D.A., 2014. Apparent directional mass-transfer capacity coefficients in three-dimensional anisotropic heterogeneous aquifers under radial convergent transport. Water Resour. Res. 50 (2), 1205–1224. https://doi.org/10.1002/2013WR014578.
Pedretti, D., Mayer, K.U., Beckie, R.D., 2017. Stochastic multicomponent reactive transport analysis of low quality drainage release from waste rock piles: controls of the spatial distribution of acid generating and neutralizing minerals. J. Contam. Hydrol. 201, 30–38. https://doi.org/10.1016/j.jconhyd.2017.04.004.
Pedretti, D., Mayer, U., Beckie, R.D., 2020. Controls of uncertainty in acid rock drainage predictions from waste rock piles examined through Monte-Carlo multicomponent reactive transport. In: Stochastic Environmental Research and Risk Assessment. https://doi.org/10.1007/s00477-019-01756-1. In press.
Peterson, H.E., 2014. Unsaturated Hydrology, Evaporation, and Geochemistry of Neutral and Acid Rock Drainage in Highly Heterogeneous Mine Waste Rock at the Antamina Mine. Peru.
Price, W.A., 2009. Prediction Manual for Drainage Chemistry from Sulphidic Geologic Materials. MEND Report 1.1 NRC Canada.
Sánchez-Vila, X., Carrera, J., 2004. On the striking similarity between the moments of breakthrough curves for a heterogeneous medium and a homogeneous medium with a matrix diffusion term. J. Hydrol. 294 (1–3), 164–175. https://doi.org/10.1016/j.jhydrol.2003.12.046.
Sharma, P.K., Ojha, C.S.P., Swami, D., Joshi, N., Shukla, S.K., 2015. Semi-analytical solutions of multiprocessing non-equilibrium transport equations with linear and exponential distance-dependent dispersivity. Water Resour. Manag. 29 (14), 5255–5273. https://doi.org/10.1007/s11269-015-1116-6.
Simunek, J., Jarvis, N.J., van Genuchten, Mth, Gärdenäs, A., 2003. Review and comparison of models for describing non-equilibrium and preferential flow and transport in the vadose zone. J. Hydrol. 272 (1–4), 14–35. https://doi.org/10.1016/S0022-1694(02)00252-4.
Skierszkan, E.K., Mayer, K.U., Weis, D., Beckie, R.D., 2016. Molybdenum and zinc stable isotope variation in mining waste rock drainage and waste rock at the Antamina mine, Peru. Sci. Total Environ. 550, 103–113. https://doi.org/10.1016/j.scitotenv.2016.01.053.
Skierszkan, E.K., Mayer, K.U., Weis, D., Roberston, J., Beckie, R.D., 2019a. Molybdenum stable isotope fractionation during the precipitation of powellite (CaMoO4) and wulfenite (PbMoO4). Geochim. Cosmochim. Acta 244, 383–402. https://doi.org/10.1016/j.gca.2018.09.030.
Skierszkan, E.K., Robertson, J.M., Lindsay, M.B.J., Stockwell, J.S., Dockrey, J.W., Das, S., Weis, D., Beckie, R.D., Mayer, K.U., 2019b. Tracing molybdenum attenuation in mining environments using molybdenum stable isotopes. Environ. Sci. Technol. https://doi.org/10.1021/acs.est.9b00766.
Smedley, P.L., Kinniburgh, D.G., 2017. Molybdenum in natural waters: a review of occurrence, distributions and controls. Appl. Geochem. 84, 387–432. https://doi.org/10.1016/j.apgeochem.2017.05.008.
Sracek, O., Choquette, M., Gélinas, P., Lefebvre, R., Nicholson, R.V., 2004. Geochemical characterization of acid mine drainage from a waste rock pile, Mine Doyon, Québec, Canada. J. Contam. Hydrol. 69 (1–2), 45–71. https://doi.org/10.1016/S0169-7722(03)00150-5.
Stollenwerk, K.G., 1995. Modeling the effects of variable groundwater chemistry on adsorption of molybdate. Water Resour. Res. 31 (2), 347–357. https://doi.org/10.1029/94WR02675.
Vriens, B., Peterson, H., Laurenzi, L., Smith, L., Aranda, C., Mayer, K.U., Beckie, R.D., 2019a. Long-term monitoring of waste-rock weathering at the Antamina mine. Peru. Chemos. 215, 858–869. https://doi.org/10.1016/j.chemosphere.2018.10.105.
Vriens, B., Smith, L., Mayer, K.U., Beckie, R.D., 2019b. Poregas distributions in waste-rock piles affected by climate seasonality and physicochemical heterogeneity. Appl. Geochem. 100, 305–315. https://doi.org/10.1016/j.apgeochem.2018.12.009.
Vriens, B., St. Arnault, M., Skierszkan, E.K., Salzsauler, K.A., Aranda, C., Mayer, K.U.K., Beckie, R.D., 2019c. Mobilization of metal(loid) oxyanions through circumneutral waste-rock drainage. ACS Omega 4, 10205–10215. https://doi.org/10.1021/acsomega.9b01270.
Willmann, M., Carrera, J., Sanchez-Vila, X., Silva, O., Dentz, M., 2010. Coupling of mass transfer and reactive transport for nonlinear reactions in heterogeneous media. Water Resour. Res. 46 (7).
Wolkersdorfer, C., Nordstrom, D.K., Beckie, R.D., Cicerone, D.S., Elliot, T., Edraki, M., Valente, T., França, S.C.A., Kumar, P., Lucero, R.A.O., Soler i Gil A., 2020. Guidance for the integrated use of hydrological, geochemical, and isotopic tools in mining operations. Mine Water Environ. https://doi.org/10.1007/s10230-020-00666-x.
Wösten, J.H.M., van Genuchten, Mth, 1988. Using texture and other soil properties to predict the unsaturated soil hydraulic functions. Soil Sci. Soc. Am. J. 52 (6), 1762. https://doi.org/10.2136/sssaj1988.03615995005200060045x.
Xu, N., Christodoulatos, C., Koutsospyros, A., Braida, W., 2009. Competitive sorption of tungstate, molybdate and phosphate mixtures onto goethite. Land Contamination & Reclamation 17 (1), 45–57. https://doi.org/10.2462/09670513.925.
Zheng, C., Bianchi, M., Gorelick, S.M., 2011. Lessons learned from 25 years of research at the MADE site. Ground Water 49 (5), 649–662. https://doi.org/10.1111/j.1745-6584.2010.00753.x.